Biosensors and Bioelectronics 141 (2019) 111347

Contents lists available at ScienceDirect

Biosensors and Bioelectronics

journal homepage: www.elsevier.com/locate/bios

Hypersensitive and selective biosensing based on microfiber interferometry and molecular imprinted nanoparticles

Anand M. Shrivastav, Gaurav Sharma, Rajan Jha*

Nanophotonics & Plasmonics Laboratory, School of Basic Sciences, Indian Institute of Technology Bhubaneswar, India

ARTICLE INFO

Keywords:
Optical sensor
Molecular imprinting
Pesticide detection
Cascaded taper fiber
Parathion methyl

ABSTRACT

The molecular imprinting techniques with interferometric platform are promising for next-generation optical sensors for online and remote biosensing and device applications. This technique has shown a tremendous potential to provide a highly specific detection of target analyte/molecule with artificial complementary scaffolds in the polymeric nanostructures relay with tunable aspect ratio, low cost synthesis procedure and applicability in harsh environment. To date, no molecular imprinted nanoparticles has been integrated with optical microwire platform in the literature. Here, we report the synthesis of a molecularly imprinted nanocarrier using hydrothermal process that act as receptors and combines optical microwire as transducing support. The detailed sensing process for one of the widely used pesticides (parathion methyl) in the detection range of 10^{-12} to 10^{-4} M with hyper-sensitivity and detection limit of 1.30×10^{12} nm/M and 79.43 fM respectively have been achieved. The compact sensing probe tested with real water samples collected from various sources show percentage recovery of around 100%. We strongly believe that the process for probe development will open a new gateway for next generation selective biosensing for biomedical research applications.

1. Introduction

Pesticides are defined as the chemical/biological substances including bacterium, virus, disinfectant, or antimicrobial which kills, deters, controls or incapacitates the pests. Parathion methyl (PM) $[(CH_3O)_2P(S)OC_6H_4NO_2]$ belongs to the organophosphorus pesticides (OPPs) family, which is widely employed for controlling the pests and due to high persistent behaviour, its residues are found in a number of agricultural species thus PM can come in contact with various living bodies and causes the adverse effects (Edwards and Tchounwou, 2005). The presence of OPPs in human nervous system result in the inhibition of the enzymatic activity of acetylcholinesterase (AChE) one which controls acetylcholine (ACh)(Eddleston et al., 2008) which acts as neurotransmitter in our nervous system whose activity is suppressed by AChE via its hydrolyzation at the rate of around 25000 molecules per second because of high catalytic activity of AChE(Quinn, 1987). Thus, OPPs can affect our nervous system anxiously and due to this, OPPs are usually termed as the neurotoxins(Cremisini et al., 1995; Guerrieri et al., 2002). OPPs irreversibly inhibit human AChE leading to the cholinergic crisis which manifests as the nicotinic, neuromuscular blockade or breath depression symptoms, and death in the case of untreated OPP intoxication (Shrivastav et al., 2016). During, their contact with skin, it may result in the involuntary muscle contractions and localized sweating(Cannard, 2006). vandDue to these adverse effects of OPPs, World Health Organization (WHO) and United States Environmental Protection Agency (US EPA) has categorized PM under 'Category la (extremely toxic)' and 'Toxicity Category I' pesticides and recommended the presence of Maximum Residual Limit (MRL) in various food stuffs ranging between 0.1 to 1 ppm (FAO/WHO, 1986;Kumar and Melo, 2015). However, several developing countries has restricted PM but it is being used in some of them (such as India) as a restricted insecticide. According to a report from the Centre of Science and Environment (CSE), India, the consumption of PM was 2739 MT (Megaton) during 2009-10 alone (CSE, 2011) which shows that it is expected to have the PM residues in the water samples, soils samples and may be in food materials. Further, the Food Safety and Standards Authority of India (FSSAI) has defined the MRL value of 0.2-1 ppm in food commodities (FSSAI, 2011, 2016). Hence, there is a strong need to develop a compact, portable, highly selective and sensitive PM detection method, which can work in harsh environment and has the potential to be used for remote and online monitoring.

The research field of optical fiber sensors have been integrated with several sensing techniques like absorbance, reflectance, Brillouin scattering, fluorescence quenching, surface plasmon resonance, luminescence etc (Kim et al., 2011; Lanticq et al., 2008; Liu et al., 2018; Marchi et al., 2017; Sharma et al., 2007) in the broad range of reports owing

* Corresponding author.
E-mail addresses: rjha@iitbbs.ac.in, rajaniitd@gmail.com (R. Jha).

https://doi.org/10.1016/j.bios.2019.111347
Received 7 March 2019; Received in revised form 17 May 2019; Accepted 21 May 2019
Available online 31 May 2019
0956-5663/

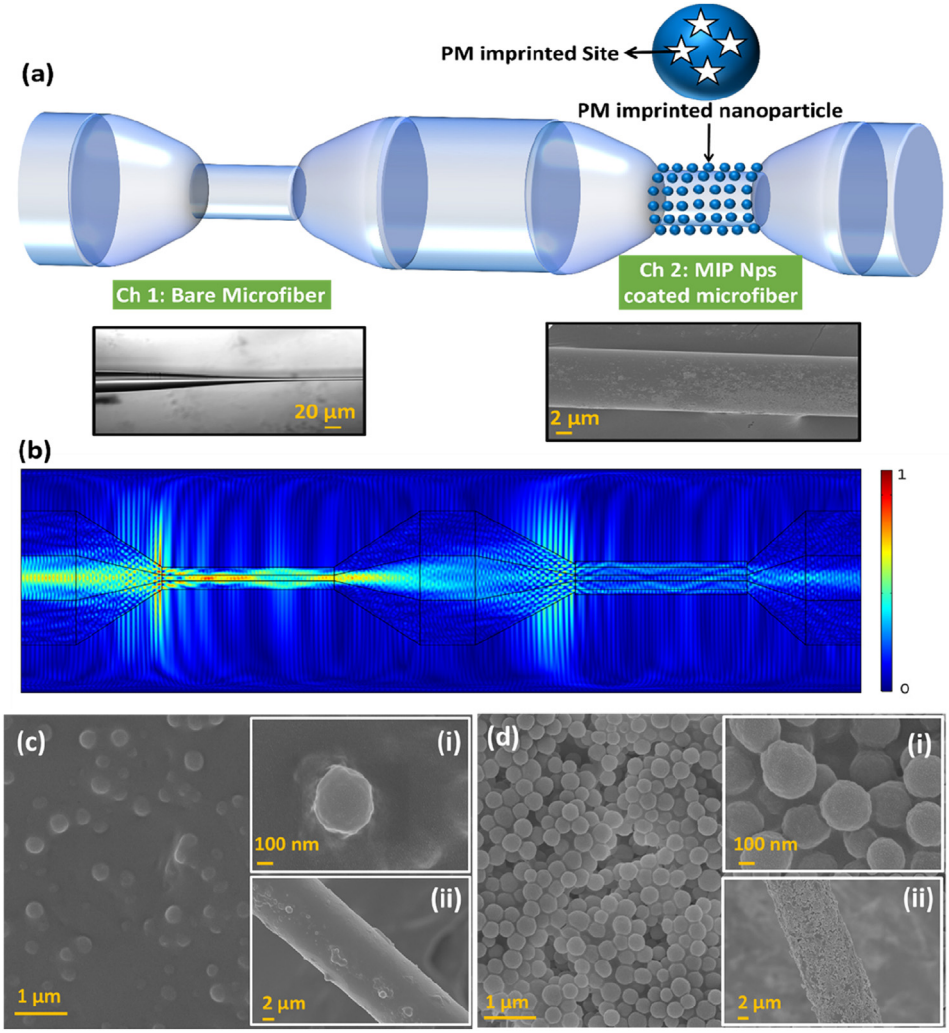

Fig. 1. (a) Schematic of proposed fabricated probe, tapered fiber images, (b) the simulated electric field distribution along the probe waist, FESEM images of (c) NIP nanoparticles and (d) MIP nanoparticles having PM imprinted sites. The (i) insets of the figures are magnified images of nanoparticle while (ii) insets are the nanoparticles coated over the fiber.

the advantages in terms of miniaturization, low cost, disposability and no electrical interference for the detection of physical, chemical and biological entities(Beard, 1998; Chien et al., 2017; DeLisa et al., 2000; Zhou et al., 2018). Among these techniques, optical fiber interferometry is one of the broadly used optical technique for making highly sensitive detection system along with high detection accuracy factor (Lee et al., 2012; Shrivastav et al., 2018). However, the sensing layer/receptor layer with high refractive index leads to the loss of interference pattern (Sharma et al., 2018). To overcome this fundamental working limitations, we are proposing concatenated tapered optical microwire that provides stable interference pattern even with high refractive index receptors. Additional noticeable advantage of the concatenated tapered microwire over single tapered optical microwire is an extra degree of freedom to tune the notch wavelength and also as single taper platform has the limitation with the operating refractive index of surrounding medium. As the refractive index of the surrounding medium is increased beyond certain value (greater than the cladding index), it result in the collapse of the interference pattern. In the dual taper platform, the first channel is used to maintain the interference pattern while the other channel will be used as working channel to achieve bio-sensing. The first channel provides the freedom to deposit the high index material over the second channel without the loss of the output interference pattern.. The interference maxima or minima in a long wavelength range is easy to select for specific wavelength with the alteration of the distance between both tapered regions (Tian et al., 2008). Further, most of the biosensing method suffers from the highly selective detection of target analytes by the sensing layer around the transducing platform. So molecular imprinting technology facilitates in developing economic synthetic receptors and acts as substitute of natural receptors such as antibodies, DNAs, enzymes, nucleic acids etc, whose synthesis are quite cumbersome and requires expert handling (Bossi et al., 2007; Hoshino et al., 2008; Vlatakis et al., 1993) and hence, several literature have referred these polymeric receptors as the “plastic antibodies” or “artificial antibodies’(Ansell et al., 1996; Cieplak and Kutner, 2016). These receptors are usually called as molecular imprinted polymers (MIPs), which have the complementary memory scaffolds of the template molecule (to be sensed) in a synthetic polymer matrix. The synthesis procedure of a generic MIP involves the co-polymerization of a functional monomer with template molecule, using the appropriate cross-linker and initiator in the subsequent solvent. After polymerization, the resultant polymer has the template molecules frozen at various places within the matrix, and these are eluted by a specific removing agent leading to the preparation of vacant template scaffolds having the potential to recognize the guest template molecule with high specificity (Cai et al., 2010; Gupta et al., 2016). Studies that have been reported where optical fiber as a platform integrated with molecular imprinting technique for biomolecule sensing (Shrivastav et al., 2016b; Cennamo et al., 2018; Usha and Gupta, 2018). However, these sensors have been

realized using plasmonic as the transducing mechanism. Additionally, as compared to MIP thin films, the nanostructured MIPs over the transducing surface possesses better sensitivity of the sensor due to increased aspect ratio that causes the more amount of analyte to interact with the imprinted sites. In view of these properties, we have proposed the MIP nanoparticles having the PM imprinted sites as the recognition medium as it leads to higher sensitivity along with the selectivity for the MIP nanostructured incorporated sensor as compared with the MIP thin films (Wackerlig and Lieberzeit, 2015).

Here, we are proposing a novel integration of microfiber based optical fiber interferometry and molecular imprinting technology for hypersensitive and selective detection of biomolecules. In the present study, concatenated tapered microwire is used for interference pattern generation and retention while molecular imprinting technique for selective detection of pesticide, e.g. parathion methyl (PM). The MIP nanoparticles are synthesized by hydrothermal polymerization method and coated over one of the dual channel microfiber platforms. Further, the sensing probe is prepared by a three-step optimization process to achieve maximum performance followed by the probe characterization with wavelength interrogation method for PM concentration range from 10^{-12} to 10^{-4} M. The specificity of the sensor is examined with respect to various other analytes belonging to PM family. The sensor's reliability is also checked by real water samples such as drinking water, tap water and ground water collected from our institute campus.

2. Numerical simulations

Fig. 1(a) shows the schematic diagram and images of taper fiber/microwire of proposed two concatenated fiber tapers of 12 mm in length each separated by 10 mm and fabricated using standard single-mode fiber (SMF-28, Corning Inc.). Simulated normalized electric field distribution in concatenated tapered fiber using COMSOL 5.2 is shown in Fig. 1(b). For simulation we have used the wavelength of incident light at 1550 nm, with cladding refractive index 1.4612, core refractive index 1.4679 and air as the background. In second tapered region a sensing layer over the tapered region is considered with refractive index 1.500. When light enters at the first down taper transition (Channel 1), the fundamental mode in SMF core will be coupled to cladding modes LP_{0m} in a degree that depends on the slope of the diameter change. At the first down taper region there is no complete recoupling from the cladding to the core mode and produces evanescent field at the slop as shown in the simulated Fig. 1(b). For up-taper region propagating core mode and excited cladding modes experience a differential phase shift that confirm the degree of interference at the up-taper transition. If transition slopes are fast enough, recoupling of cladding to core mode remains incomplete and some light remains propagating through the cladding. Interesting part of the output spectrum of this concatenated tapered microwire is spectral modulation with periodically separated notch and their period depends inversely on the separations between the tapered regions.

The interference equation of the fundamental core mode and the cladding mode is expressed as Eq. (1).

$$I = I_1 + I_2 + 2\sqrt{I_1 I_2}\cos\varnothing \quad (1)$$

Where $\varnothing$ is the phase difference ($\varnothing = 2\pi\Delta n_{eff} L/\lambda$) between modes, I_1 and I_2 are the light intensity of the fiber core fundamental mode and the lowest order cladding mode, respectively. Δn_{eff} is the difference of the effective refractive index between the interfering modes, λ is the input wavelength. Phase difference condition$\varnothing = (2m + 1)\pi$, m = 0, 1, 2 …,. The intensity of interference reaches minimum value, spectrum wavelength dip can be expressed as $\lambda_m = 2\Delta n_{eff} L/(2m + 1)$. The spacing between the adjacent dip wavelengths is given by $\Delta\lambda = \lambda_m - \lambda_{m-1}$. When the refractive index surrounding the waist region (channel 2) increases by δn, which enhances the effective refractive index of the cladding mode although core mode it is nearly constant. Hence, Δn_{eff} increases and causes the shift in interference spectrum dip wavelength λ_m towards shorter value. This shift can be expressed as $\delta\lambda_m = 2\delta n_{eff} L/(2m + 1)$. Further, the concatenated tapered region also plays a role for the wavelength shift, which can be represented by $\delta\lambda_p = 2\delta n_{eff} L'/(2p + 1)$, where L' is the distance between the centers of the tapered region. Further, the wavelength sensitivity of the concatenated tapered region will be increased by the increasing the separation between the centers of both the tapered region (Tian et al., 2008; Wang et al., 2016).

It may be noted that Fig. 1(b) depict the electric field distribution around the probe (channel 1 and channel 2) and shows that probe is wavelength sensitive to change in surrounding refractive index. This sensitivity is largely affected by evanescent field of the tapered fiber and therefore the knowledge of electric field distribution is important for sensing at large (Sharma et al., 2019; Huntington et al., 1999).

3. Fabrication of probe

3.1. Preparation of concatenated microfiber platform

The fiber optic sensing platform is fabricated by tapering the fiber using an automated robotic tapering system operated via flame and burst technique at two different positions(Dass and Jha, 2015). The diameter and waist of the tapered fiber (microfiber) of both the positions are kept as 10 μm and 12 mm respectively. The distance between both the channels is maintained as 10 mm. The first tapered waist is termed as channel 1 while the second one is named as channel 2 respectively. Channel 1 is used as the reference channel to maintain the interference pattern and channel 2 is employed as the sensing channel. Further, MIP nanoparticles (sensing medium) using PM as template molecule are synthesized and layered over the channel 2 microfiber.

3.2. Synthesis of MIP nanoparticles

For the synthesis of PM imprinted nanoparticles, initially, a pre-polymerization complex is prepared by mixing 0.025 M PM (Parathion Methyl, template) and 0.1 M MAA (Methacrylic Acid, functional monomer) in 5 ml CAN (Acetonitrile, solvent) for 2 h via ultrasonication followed by the addition of 0.1 M EGDMA (Ethyleneglycol dimethacrylate, cross-linker) and 0.065 gm AIBN (2, 2-azobis-isobutyronitrile, reaction initiator) in the solution. The pre-polymerization self-assembly is thermally polymerized in an oven at 60 °C for 6 h. To obtain the polymerized complex having PM molecules fixed within the domains of the polymer. This polymer is named as non-imprinted polymer (NIP). The NIP polymer is coated over the channel 2 of fabricated fiber optic platform via physical adsorption method. In this method, the microfiber region of channel II is washed thoroughly with acetone and methanol followed by the piranha solution to remove contaminations over the fiber surface. Then, the fiber is kept at 70 °C for two hours. The tapered regime is dipped in the NIP solution in a lab made customized system for 30 min so that NIP nanoparticles can immobilized efficiently over the fiber surface through physical adsorption. The fiber optic probe is then removed from the NIP polymer solution and finally left for drying at 70 °C in oven for two hours. Now, the PM imprinted sites in the NIP coated fiber surface are created by dipping the channel 2 in acetonitrile and ethanol (9:1, v/v) solution for 15 min followed by drying the probe in nitrogen gas environment that leads the MIP nanoparticle coated over the microfiber platform. This completed the probe fabricated process. The FESEM images of NIP and MIP nanoparticles and their coatings over the fiber optic surface has been shown in Fig. 1 (c) and (d) respectively.

4. Sensing mechanism

The sensing operation of the advance fabricated probe recognize the change in the effective index of sensing layer i.e. MIP nanoparticle layer due to binding of guest PM molecules with the PM imprinted voids. PM

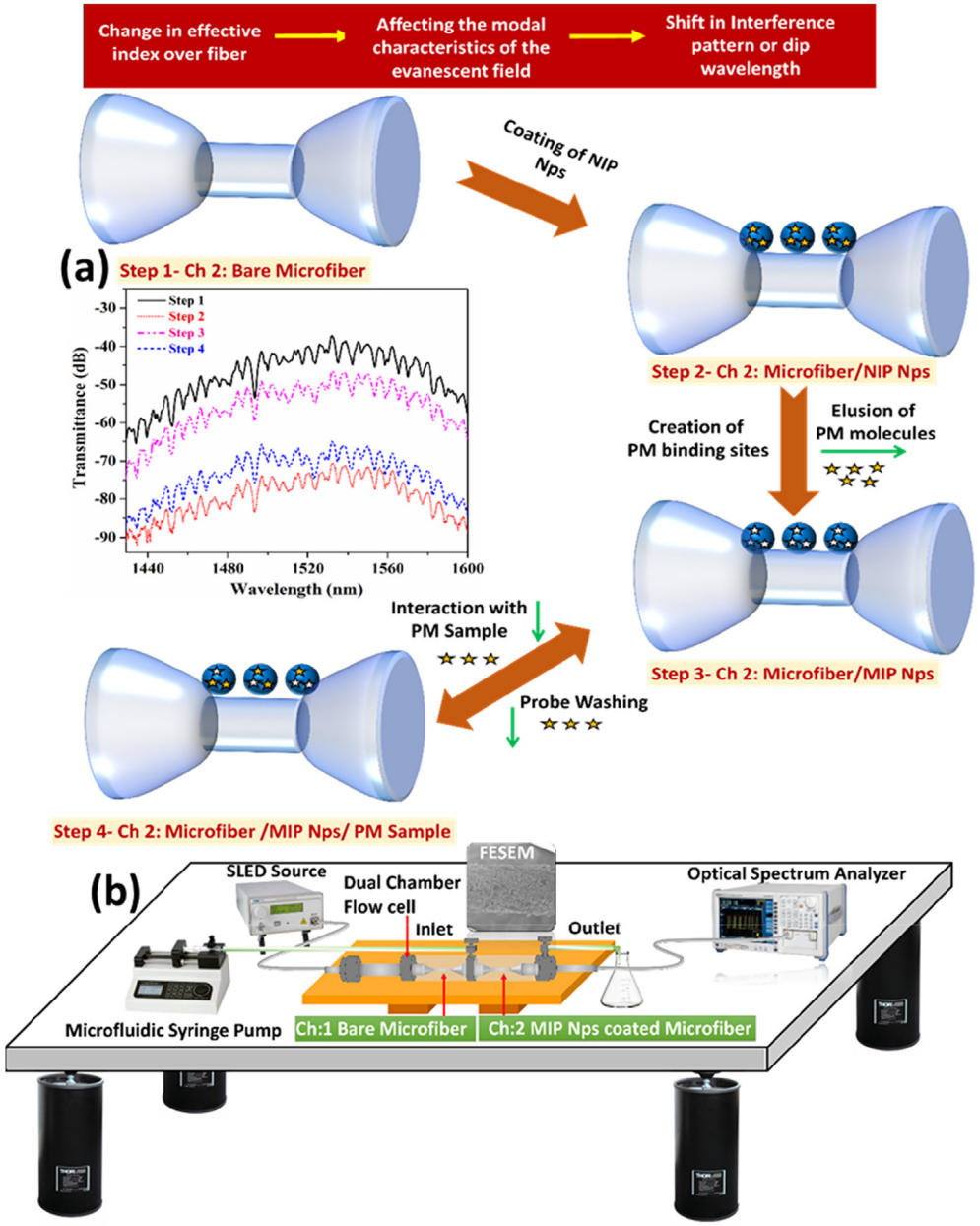

Fig. 2. (a) Different probe fabrication steps and corresponding interference spectrum with various probe configurations to validate PM sensing and (b) Proposed experimental set-up for the characterization of the probe.

molecules of guest aqueous samples interact with the imprinted sites in MIP nanoparticles and locked inside due to the complementary shape and size along with the hydrogen bonding between the template (PM) and the monomer methacrylic acid (MAA). Interactions between these molecules with time causes change in effective index of MIP nanoparticle layer and modulates cladding modes that causes the wavelength and intensity shift in transmitted interference pattern. Thus, by monitoring this shift, we can find the presence of PM concentration in the aqueous solution. To validate the proposed sensing mechanism, we have performed the control experiments which also shows the effect of each step during the probe fabrication process. Fig. 2 the probe fabrication/sensing steps and corresponding modulation in interference patterns with various probe configurations respectively. To prepare the probe, in first step we fabricated the concatenated tapered optical fiber using flame and brush technique. Corresponding interference pattern has been shown as solid lined spectrum in the figure. In next step, we coated the NIP nanoparticles (polymeric nanoparticles having PM molecules in their domains) over channel 2 and corresponding interference pattern is given in red dotted line. As compared to spectrum obtained in step 1, this interference pattern gets changed in terms of more power loss and as well as the shift in wavelength due to the presence of high dielectric medium over the tapered region. In the third step, during the probe fabrication, the elution of PM molecule is performed which leads to the decrease in the effective index of the medium surrounding the channel 2 of the optical fiber platform. In this scenario, the channel 2 (Microfiber/MIP nanoparticle) shows less loss in the interference pattern with respect to that of step 2 which is represented by pink dash-dotted curve. Now, to execute sensing, the aqueous PM sample is inserted in channel 2 of flow-cell (shown in Fig. 2 (b)) by microfluidic syringe. As the PM molecule interacts with the MIP nanoparticle, the effective index of the sensing layer again changes and causes the wavelength shift and propagation loss in the interference pattern due to their non-covalent bonding which is observed as blue dashed interference pattern in Fig. 2 (Step 4). The material used, probe

fabrication process and the experimental setup have been briefly discussed in Supplementary Materials.

5. Results and discussions

5.1. Optimizations of probe parameters

In order to achieve the best performance of the fabricated probe a three-stage optimization process is performed: the concentration of PM molecule for the synthesis of MIP nanoparticles, the dipping time for the NIP nanoparticle coating and the elusion time for PM molecules from the polymer layer. There are several parameters which affect the sensor's performance such as template concentration, solvent concentration, crosslinking agent concentration, polymerization time etc. Among them, three parameters have been optimized as these parameters play an important on the activity of MIP layer and the optimization stages are selected in a manner that the parameter which affects the probe maximum is optimized first. The main parameter which decides the sensor's activity is the number of recognition sites in the MIP nanoparticle layer (sensing layer) which is decided by the concentration of PM molecules in the MIP during probe synthesis. This is optimized in the first step while the second step decides the thickness which is basically related to the interaction of evanescent field with the sensing layer and hence affect the sensitivity of the probe. The third step (optimization of removal time for NIP to MIP formation) results the effective removal of PM molecules for the creation of binding sites without changing the shape and size of recognition sites. Further, since all the optimizations cannot be performed in one step, so we decided to optimize one keeping other two fixed at certain values which are selected at a specific value. Now, these are discussed below:

5.1.1. Optimization of PM concentration for MIP nanoparticle synthesis

The amount of template molecule used for the synthesis of MIPs is one of the most important factors affecting the performance of a sensing unit. It decides the numbers and as well as the structure of the artificial binding sites for the interaction with the guest PM molecules. Thus, for the experiments MIP nanoparticles with varying PM concentrations from 10 to 35 mM are synthesized and used for probe fabrication while the dipping time of NIP polymer coating and removal time are maintained as 20 min and 30 min respectively. The fabricated probes are experimented using the setup, (as shown in Fig. 2(b)), with aqueous PM samples having concentrations 0 and 10^{-4} M and corresponding shifts in specific dip wavelength of the interference patterns for each probe is recorded. In the experimental set-up, light is launched from SLED (Thor labs, S3FC1550) source and its corresponding transmitted spectrum is collected by the optical spectrum analyzer. The obtained interference plots using the probe fabricated with various PM concentration in MIP nanoparticle synthesis keeping the dipping time for MIP nanoparticle coating and removal time for leaching templates fixed are shown in Supplementary Fig. S1. Fig. 3(a) represents the change in dip wavelength with varying PM concentrations used for the probe fabrication which depicts that for 25 mM concentration, the maximum shift of 4.5 nm in dip wavelength is observed. This is because of the concentration of template molecules which decides the number of imprinted/binding sites for the recognition. For lower PM concentration, the number of binding sites will be less while for higher concentration of PM, the shape of the binding scaffolds will be disturbed due to the finite surface area over the microfiber region. Hence, in both the cases a smaller number of guest PM molecules can bind with the sensing layer which will lead the lesser shift in dip wavelength respect to the optimized PM concentration (25 mM).

5.1.2. Optimization of dipping time for NIP nanoparticle coating

The dipping time for the polymeric nanoparticle coating is optimized since it deflects the thickness of the sensing layer for the fabricated probe. The thickness of the sensing layer decides the sensor's performance as the film thickness decides the electric field intensity of higher order mode at the sensing region affecting the sensitivity of the probe (Shrivastav et al., 2017). Hence, the probes with varying dipping time for the NIP nanoparticle coating are prepared with varying dipping times from 10 to 50 min keeping the template concentration of 25 mM and template removal time of 10 min. The interference patterns recorded with different probe configurations has been shown in Supplementary Fig. S2. The spectra are recorded for the guest PM solutions with concentration 0 and 10^{-4} M. Fig. 3(b) shows the change in dip wavelength with different dipping periods for the probe fabrication showing the maximum shift in dip wavelength is around 5 nm for the 30 min dipping period. The one reason for this optimized value has been discussed above. Additionally, for lower thickness of the sensing layer, there will be a smaller number of binding sites due to fewer loading of nanoparticles while the thicker film of nanoparticle layer may lead the binding of most target PM molecules at the sensing layer-analyte surface (far from the microfiber surface), where electric field intensity of the evanescent wave will be less. In both the cases, the shift in dip wavelength will be less compared to the optimized value of dipping time. The optimized dipping time for the NIP nanoparticle coating is obtained as 30 min showing the shift in dip wavelength of 5 nm.

5.1.3. Optimization of the removal time for the creation of PM imprints

The final stage of probe optimization process is the removal time for creating PM imprinted sites in NIP nanoparticle coated over the channel II of the probe. This is done by dipping the NIP coated probes in acetonitrile and ethanol (9:1, v/v) solution for varying time periods of 5–25 min. In this case, the PM concentration for nanoparticle synthesis and dipping time for nanoparticle coting is used as 25 mM and 30 min respectively, which are the optimized values, obtained from the previous stages. Fig. S3 shows the probe response prepared with different leaching time for creation of imprinted sites and correspondingly, Fig. 3(c) depicts that the best performance of the sensor is found for 10 min removal time showing the shift in dip wavelength of 6.0 nm. The removal time of less than 10 min is not enough to remove all PM molecules to create binding imprints while for higher removal time affecting the MIP nanoparticle film. This completed the probe optimization steps with the various optimized parameters including PM concentration for MIP nanoparticle synthesis (25 mM), the dipping time for nanoparticle coating (30 min) and removal time of PM molecules for the creation of PM imprints (10 min). The error bars shown in Fig. 3(a–c) shows the standard deviation in dip wavelength change while performing the experiments up to 10 times.

5.2. Probe characterization

After the optimization process, the final probe is used for the characterization. Aqueous PM samples with varying concentrations from 0 to 10^{-4} M is inserted successively in the flow cell using microfluidic syringe and for each sample, the transmitted spectra are recorded. Fig. 4(a) shows the interference spectra for each sample with tracking a specific dip wavelength concluding that interference spectrum shifts towards the lower wavelength regime as PM concentration of the aqueous sample increases. The shift is due to the change in effective index of the sensing layer by the binding of PM molecules with the complementary imprints present in the nanoparticle layer. During the probe characterization process, the sensing probe is washed with De-ionized water between two consecutive measurements to detach any bound/unbound PM molecules before loading the next guest PM sample solution to remove any essence of the previous solution. The bound guest PM molecules with the binding sites are usually interacts with the physical adsorption at the imprinted sites and weak non-covalent bond that is easy broken with water molecules during the washing the probe. Now, for the calibration of the probe, a specific interference dip and corresponding dip wavelength was chosen, and it was traced with

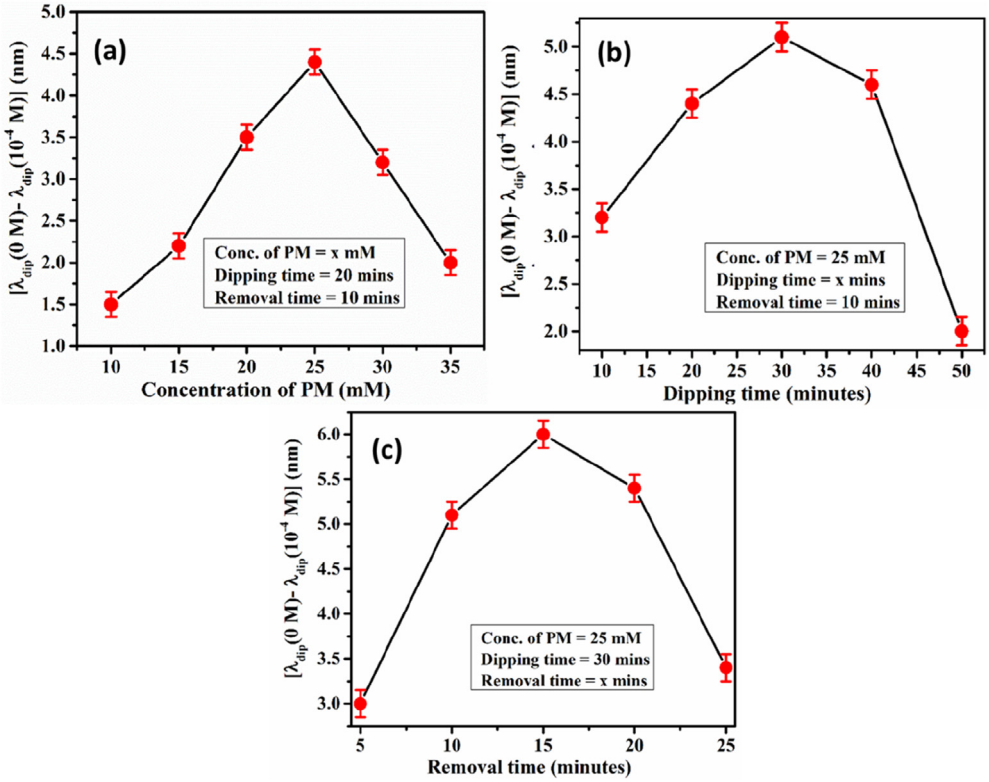

Fig. 3. Optimizations plots for (a) PM (template) concentration used for MIP nanoparticle synthesis, (b) dipping time for NIP nanoparticle coating and (c) removal time for the creation of PM imprints.

consecutively varying concentration of PM solutions in the flow cell. Now, the sensing probe is calibrated by plotting the change in dip wavelength as a function of PM concentration, shown in Fig. 4(b). Further, each cycle of probe characterizations has been repeated up to ten times and standard deviation in the dip wavelength change for each concentration of PM solution is plotted as the error bars in the calibration curve (Fig. 4(b)). The calibration curve represents the shift in dip wavelength of 5.4 nm with PM concentration change from 10^{-12} M to 10^{-4} M while for the concentration change of 0 M to 10^{-4} M PM solutions, the shift in dip wave length is 6.0 nm. The calibration curve is fitted by a second order polynomial as following relation:

$$\Delta\lambda = 4.375 - 0.555 \times (\log C) - 0.0772 \times (\log C)^2 \quad (2)$$

The figure also concludes the saturation behavior for the higher concentration of PM solution, which is due to the limited number of recognition sites in the MIP nanoparticle layer that results the decrease in available binding site per PM molecule as the sample concentration increases. Further, the sensitivity dynamics of the probe is calculated by taking the derivative of the calibration relation of the probe as following relation:

$$S = \frac{\partial(\Delta\lambda)}{\partial C} = -\frac{1}{C}[0.555 + 0.1544 \times (\log C)] \quad (3)$$

The calculated values of sensitivities from the above equation are 1.30×10^{12}, 1.41×10^{11}, 9.89×10^{9}, 8.35×10^{8}, 6.80×10^{7}, 5.26×10^{6}, 3.71×10^{5}, 2.17×10^{4}, 6.26×10^{2} nm/M at PM concentrations of 10^{-12}, 10^{-11}, 10^{-10},10^{-9} ,10^{-8} ,10^{-7} ,10^{-6} ,10^{-5} and 10^{-4} M respectively. For the sake of convenience, the logarithms of the obtained sensitivity values are plotted in Fig. 4(c) and a linear relationship with the logarithm of the PM concentrations has been found as following equation with the R^2 values of 0.99.

$$\log S = -1.426 - 1.141 \times (\log C) \quad (4)$$

A decrease in sensor's sensitivity is found for increase in the concentration of PM sample solution. Further, the detection limit of the proposed method is calculated using calibration equation considering the third time of standard deviation in the dip wavelength (from Fig. 4(b)) which provides the detection limit of 7.943×10^{-14} M (79.43 fM). Further, it is to be noted that the proposed method can also be calibrated as the change in the transmitted power of output light. However, we have preferred the wavelength interrogation method because any fluctuations in the light propagating through the fiber due to the fiber bending, decoupling or variation of the light in the input source power may alter the light intensity and then based on the intensity based calibration, the output data may predict the incorrect PM concentration in the aqueous sample solution.

5.2.1. Selectivity

The selectivity of a sensing device is a parameter which decides whether the device responses only for the desired analyte or various other analytes belonging to the same family or the analytes which intercepts the sensor's performance. The analytes chosen for the selectivity experiments are parathion methyl (PM), parathion, paraoxon, fenitrothion because these have quite similar molecular structure/functional groups, as seen from Fig. 4(d). The aqueous samples of these analytes with concentrations of 10^{-4} M are prepared and the optimized probe is characterized with these samples. Fig. 4(d) shows the bar representation of the observed change in dip wavelength for these samples with dip wavelength with de-ionized water (0 M). From figure, it can be said that the probe showed the maximum shift only for PM samples as compared to other analytes. This is because of the presence of complementary PM sites in the MIP nanoparticle layer which limits the binding of any other molecules having different structure and functional group with the sensing layer. The probe with NIP nanoparticle layer is also experimented with these samples and a fewer shifts in dip wavelength for all the samples is observed as shown in the figure. This also confirms the high selectivity of the probe is only due to the imprinted sites.

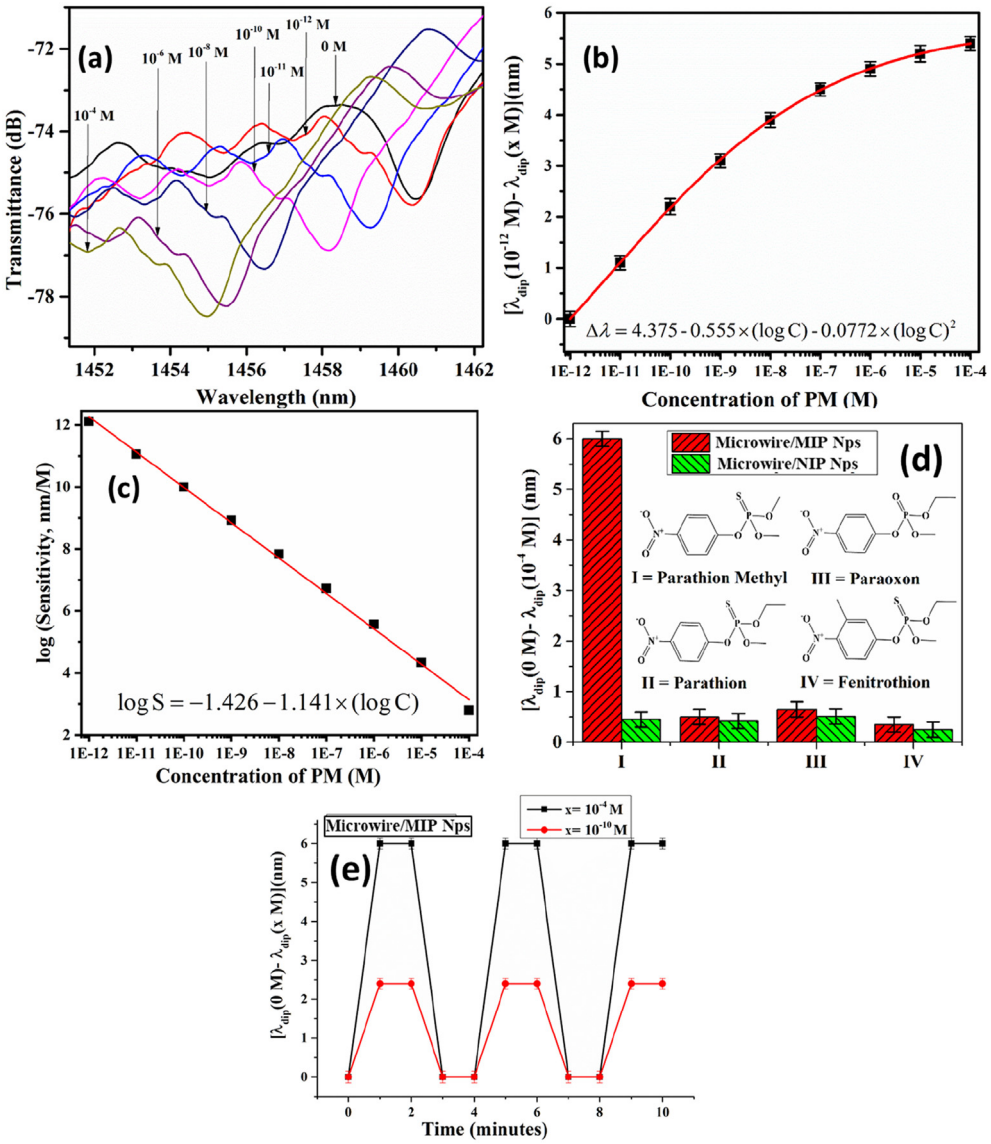

Fig. 4. (a) Probe characteristic plot, (b) calibration curve, (c) sensitivity, (d) selectivity and (e) repeatability and stability dynamics of proposed probe having configuration: Dual taper/MIP Nps with the optimized parameters.

5.2.2. Repeatability and stability

Repeatability and stability of the fabricated probe is examined with two PM samples with concentrations of 0 and 10^{-4} M. Initially, 0 M PM sample is inserted in the flow cell and the interference spectrum is collected by OSA. The sample is then removed from flow cell and 10^{-4} M PM sample is poured in the flow cell and interference pattern is recorded after 1 min so that sample can effectively interact with the probe. The sample is then left in the flow cell and after 1 min the pattern is again recorded for stability examination. Now, 10^{-4} M PM sample is removed, and the probe is washed with de-ionized water to remove any bound/unbound guest PM molecules of the previous sample. Further, 0 M PM sample is again injected in the flow cell and corresponding interference output is collected. The removing of 10^{-4} sample from the flow cell, the washing of the probe and the injection of 0 M PM sample takes about 1 min 0 M PM solution is again retained for 1 min in the flow cell and after that the interference pattern is collected. Thus, first cycle of the experiment is completed. The repeatability of the probe is checked by performing these cycles several times. From collected interference spectra, change in a specific dip wavelength corresponding to 0 M PM solution is traced and plotted as Fig. 4 (e). The experiments are also conducted on the same probe and as well as on freshly prepared probe which shows a good repeatability and stability performance of the sensor as the change in the data points lies within the error bar values in the calibration plot of the sensing probe (Fig. 4(b)). The repeatability of the optimized probes is also performed with the 10^{-10} M PM solution as discussed above, the probe applicability for the lower concentrations of the sample solutions also shows a good response as shown in Fig. 4(e). It may be noted that, when few cycles of repeatability experiments are completed, the probe is washed with DI water to remove all unwanted guest PM molecules and then kept in a plastic box to prevent the probe from the atmospheric contaminants for several days at room temperature. The repeatability experiment is again performed in the similar manner as performed for the fresh probe. The results with in the acceptable error range confirms the long-term stability, high shelf life and industrial applicability of the probe.

In addition, a comparison of several performance parameters for various other PM detection methods reported in literature are also made in Table 1 to find the advantages of our methods above several studies. It can be concluded that the present reported method possesses the lowest limit of detection value to best of our knowledge and this will opens a completely new window for selective biosensing by

Table 1
Comparison of various analytical parameters for PM detection using the proposed methods with previously reported studies.

Method (Reference)	Sensor Configuration	Interrogation Method	Dynamic Range	Linear Range	Sensitivity	Detection Limit	Practical Application
Mass-Sensitive (QCM) Cheng et al. (2017)	MIP/Quartz Crystal	Frequency	0–100 μM	0–100 μM	–	8.3×10^{-7} M	Water samples
Electrochemical (Zhang et al., 2012)	MIP-MWCNT/GCE	CV	2.0×10^{-7} -1 x 10^{-5} M	2.0×10^{-7} -1 x 10^{-5} M	0.4269 μA/μM	6.7×10^{-8} M	Pear and Cucumber Samples
Electrochemical (Wang et al., 2018)	MIP/Au/GCE	CV	0–15 μM	0–1 μM 1–15 μM	1.281 μA/μM-cm^2 0.3325 μA/μM-cm^2	5×10^{-8} M	Water, Fruit Juice and Vegetable Samples
Electrochemical (Rahmani et al., 2018)	BSA templated Au–Ag nanoclusters/GCE	SWASV	0–200 μM	0.02–8 μM 8–200 μM	2.036 μA/μM 0.6041 μA/μM	8.2×10^{-9} M	Water, Vegetable, Apple and Soil Samples
Electrochemical (Song et al., 2016)	Nano-TiO_2 graphene composite/GCE	CV & LSV	0–100 μM	0.002–5 μM 5–100 μM	4.9565 μA/μM 0.8206 μA/μM	1×10^{-9} M	Apple Samples
Optical (Mishra et al., 2017)	*Sphingomonas* sp. Cells immobilized silica Nps	Absorbance	0–1 ppm	0.1–1 ppm	0.0443 A.U./ppm	0.1 ppm (3.4×10^{-10} M)	Water and Grapes Samples
Electrochemical (Govindasamy et al., 2017)	Ag@Graphene nanoribbons/ SPCE	Amperometry	0.005–2780 μM	0.005–2780 μM	0.5940 μA/μM-cm^2	0.5 nM	Vegetables and Fruit Samples
Electrochemical (Tian et al., 2018)	CuO–TiO_2/GCE	CV	0–2000 ppb	10–500 ppb	0.0412 A.U./ppb	1.21 ppb (5.0×10^{-10} M)	Ground Water Samples
Electrochemical (Li et al., 2018)	Surface MIP microsphere/GCE	CV & ESI	1×10^{-12} – 8×10^{-9} M	1×10^{-12} – 8×10^{-9} M	8.715 μA/(ln M)	3.4×10^{-13} M	Soil and Vegetables
Electrochemical (Wu et al., 2014)	MIP-MWCNT/Au Nps/GCE	CV & ESI	0–11 ng/ml	0.1–1.1 ng/ml 1.1–11 ng/ml	12.35 μA/ng-mL^{-1} 6.3395 μA/ng-mL^{-1}	0.08 ng/ml (2.7×10^{-13} M)	Water, Apple and Cucumber Samples
Plasmonics (SPR) Tan et al. (2015)	MIP/Au/Glass Chip	Angular Interrogation	10^{-13}- 10^{-10} M	10^{-13}– 10^{-10} M	0.036 deg/logM	10^{-13} M	–
Interferometric (Present Study)	MIP Nps/Dual Taper Microwire	Wavelength Interrogation	10^{-12}-10^{-4} M	–	1.30×10^{12} nm/M @10^{-12} M	7.94×10^{-14} M	Water Samples

BSA = Bovine Serum Albumin; CV = Cyclic Voltammetry; EIS = Electron Impedance Spectroscopy; GCE = Glass Carbon Electrode; LSV = Linear sweep Voltammetry; MWCNT = Multi-wall Carbon Nanotubes; Nps = Nanoparticles; SPCE = Screen Printed Carbon Electrode; SWASV = Square Wave Anodic Stripping Voltammetry.

Table 2
Detection of PM in water samples collected from various resources.

Sample	Spiked PM (M)	Found PM concentration by our method (M)	% Recovery
Drinking water	1×10^{-8}	0.983×10^{-8}	98.3
	1×10^{-6}	0.978×10^{-6}	97.8
	1×10^{-4}	0.98×10^{-4}	98.0
Tap water	1×10^{-8}	1.015×10^{-8}	101.5
	1×10^{-6}	0.992×10^{-6}	99.2
	1×10^{-4}	1.02×10^{-4}	102.0
Ground water	1×10^{-8}	1.008×10^{-8}	100.8
	1×10^{-6}	1.01×10^{-6}	101.0
	1×10^{-4}	1.012×10^{-8}	101.2

integrating the optical interferometry and molecular imprinting technology.

5.2.3. Real sample analysis

To find the sensor's applicability for the food and agricultural applications, the sensing probe is characterized by the various water samples including drinking water, tap water and ground water collected from the IIT Bhubaneshwar campus. Initially, these samples are characterized with conventional GC-MS method for the benchmarking (Li et al., 2010). The method showed the operating range for PM detection of 0.1–25 μg/l (3.43×10^{-10}-8.58×10^{-8} M). Additionally, the method possessed the LOD value of 32.2 ng/l (1.105×10^{-10} M). Now, to examine the sensor's performance, the PM with varying concentrations of 1×10^{-8} M, 1×10^{-6} M and 1×10^{-4} M are prepared in the same water samples. The optimized probe is characterized with these PM sample solutions. For each solution, shift in the interference dip wavelength has been recorded with respect to the dip wavelength observed for that of DI water (reference solution used for the probe characterization). Further, for each sample, the PM concentration is evaluated using the calibration equation, which has been shown in Table 2. Now, in order to evaluate the probe performance, we calculated the % recovery as following equation:

$$\% \text{ Recovery} = \frac{\text{Observed PM concentration from the proposed method}}{\text{Acutal PM concentration of the sample solution}} \times 100$$

The table concluded that the % recovery of the sensor lies within the range of 97.8%–101.2% which confirms that our sensing method possessed the potential to work with real samples. However, Table 2 depicts that the observed value of PM concentration is a bit different from the actual value of PM concentration which was higher (in some cases) than the actual concentration of PM in the sample solution resulting the %recovery more than 100%. This is because of various experimental instrumentational error and probe handling process.

It may be noted that the proposed fiber optic probe possesses the novelty on the basis of the integrated molecular imprinted nanoparticles with the concatenated tapered based microwire platform. The proposed optical microwire platforms has been reported earlier in various studies for realization of inline Mach–Zehnder Interferometric sensor (Sharma et al., 2019) and refractive index sensor (Tian et al., 2008; Wang et al., 2016) but the molecular imprinting technique for biomolecule sensing has been never reported before this communication to the best of our knowledge which is the novelty of the proposed work. Additionally, this integration has the advantage of the highly sensitive detection system along with high detection accuracy (due to the interferometric platform) and the freedom to select the operating wavelength with the molecular imprinting technique provides the highly selective detection of the biomolecules with ease of synthesis, handling procedure and the cost-effectiveness as compared to the conventional receptors such as enzymes, antibodies etc (Gupta et al., 2016).

6. Conclusion

A contemporary approach for the biosensing applications has been reported utilizing a implementation of molecular imprinting technology and optical fiber interferometry has been proposed. PM imprinted nanoparticles are synthesized by hydrothermal process that acts as the artificial receptors while concatenated optical microwire is used as transducing platform. The proposed sensing probe is fabricated through a three-stage optimization process while the sensor probe is characterized for PM concentration of 10^{-12} to 10^{-4} M. The sensing probe possesses the sensitivity of 1.30×10^{12} nm/M and the detection limit of LOD as 7.943×10^{-14} M (79.43 fM) that can be further enhanced by probe and system optimization. The performance of the probe with real water samples depicted the sensor's applicability for industrial and agricultural applications. This unique integration of optical fiber interferometry and nanosized molecular imprinted polymers offers a unique platform for highly sensitive biosensor with selective biomolecules detections for broad range of applications.

Declaration of interests

The authors declare that they have no known competing financial interests or personal relationships that could have appeared to influence the work reported in this paper.

The authors declare the following financial interests/personal relationships which may be considered as potential competing interests.

Rajan Jha (on behalf of all authors)

CRediT authorship contribution statement

Anand M. Shrivastav: Formal analysis, Data curation, Writing - original draft, Writing - review & editing. **Gaurav Sharma:** Formal analysis, Software, Validation, Writing - original draft, Writing - review & editing. **Rajan Jha:** Project administration, Supervision, Writing - review & editing.

Acknowledgements

This work is partially supported by MHRD funded project CENEMA, DST funded project EMR/2016/003446 and also ISRO funded project ISRO/RES/3/757/17-18. GS thanks SERB for NPDF-2017/0529.

Appendix A. Supplementary data

Supplementary data to this article can be found online at https://doi.org/10.1016/j.bios.2019.111347.

References

Ansell, R.J., Ramström, O., Mosbach, K., 1996. Clin. Chem. 42 (9), 1506–1512.
Beard, P.C., 1998. Opt. Lett. 23, 1235–1237.
Bossi, A., Bonini, F., Turner, A.P.F., Piletsky, S.A., 2007. Biosens. Bioelectron. 22, 1131–1137.
Cai, D., Ren, L., Zhao, H., Xu, C., Zhang, L., Yu, Y., Wang, H., Lan, Y., Roberts, M.F., Chuang, J.H., Naughton, M.J., Ren, Z., Chiles, T.C., 2010. Nat. Nanotechnol. 5, 597–601.
Cannard, K., 2006. J. Neurol. Sci. 249, 86–94.
Cennamo, N., D'Agostino, G., Porto, G., Biasiolo, A., Perri, C., Arcadio, F., Zeni, L., 2018. Sensors 181 (6), 1836.
Cheng, X., Zhang, Q., Li, S.F.Y., Liu, B., 2017. Malaysian J. Anal. Sci. 21, 1327–1334.
Chien, P.J., Suzuki, T., Tsujii, M., Ye, M., Toma, K., Arakawa, T., Iwasaki, Y., Mitsubayashi, K., 2017. Biosens. Bioelectron. 91, 341–346.
Cieplak, M., Kutner, W., 2016. Trends Biotechnol. 34 (11), 922–941.
Cremisini, C., Di Sario, S., Mela, J., Pilloton, R., Palleschi, G., 1995. Anal. Chim. Acta 311, 273–280.
CSE, 2011. Centre of science and environment (CSE). State of pesticide regulations in India. Available from: http://www.cseindia.org/userfiles/paper pesticide.
Dass, S., Jha, R., 2015. IEEE Photonics Technol. Lett. 28, 31–34.
DeLisa, M.P., Zhang, Z., Shiloach, M., Pilevar, S., Davis, C.C., Sirkis, J.S., Bentley, W.E.,

2000. Anal. Chem. 72, 2895–2900.
Eddleston, M., Buckley, N.A., Eyer, P., Dawson, A.H., 2008. Lancet 371, 597–607.
Edwards, F., Tchounwou, P., 2005. Int. J. Environ. Res. Public Health 2, 430–441.
FAO/WHO, 1986. Codex Alimentarius Commission CAC, third ed. vol. XIII Food and Agriculture Organization of the United Nations, Rome.
FSSAI, 2011. Food Safety and Standards (Contaminants, Toxins and Residues) Regulations. http://www.fssai.gov.
FSSAI, 2016. Fixation of MRLs for pesticide residues in processed foods. Modalities. http://fssai.gov.
Govindasamy, M., Mani, V., Chen, S.M., Chen, T.W., Sundramoorthy, A.K., 2017. Sci. Rep. 7, 1–11.
Guerrieri, A., Monaci, L., Quinto, M., Palmisano, F., 2002. Analyst 127, 5–7.
Gupta, B.D., Shrivastav, A.M., Usha, S.P., 2016. Sensors 16, 3181.
Hoshino, Y., Kodama, T., Okahata, Y., Shea, K.J., 2008. J. Am. Chem. Soc. 130, 15242–15243.
Huntington, S.T., Katsifolis, J., Moar, P.N., Roberts, A., Cahill, L.W., Nugent, K.A., 1999. IEE Proc. - Optoelectron. 146 (5), 239–243.
Kim, Y.H., Kim, M.J., Rho, B.S., Park, M.S., Jang, J.H., Lee, B.H., 2011. IEEE Sens. J. 11, 1423–1426.
Kumar, J., Melo, J.S., 2015. Advances in Biosensors Research. Nova Science Publishers, Inc, pp. 89–112 978–1-63463–652-0.
Lanticq, V., Quiertant, M., Merliot, E., Delepine-Lesoille, S., 2008. IEEE Sens. J. 8, 1194–1201.
Lee, B.H., Kim, Y.H., Park, K.S., Eom, J.B., Kim, M.J., Rho, B.S., Choi, H.Y., 2012. Sensors 12, 2467–2486.
Li, X., Gan, P., Peng, R., Huang, C., Yu, H., 2010. J. Chromatogr. Sci. 48 (3), 183–187.
Li, Y., Liu, J., Zhang, Y., Gu, M., Wang, D., Dang, Y. yan, Ye, B.C., Li, Y., 2018. Biosens. Bioelectron. 106, 71–77.
Liu, D., Kumar, R., Wei, F., Han, W., Mallik, A.K., Yuan, J., Yu, C., Kang, Z., Li, F., Liu, Z., Tam, H.Y., Farrell, G., Semenova, Y., Wu, Q., 2018. J. Light. Technol. 36, 3672–3677.
Marchi, G., Baier, V., Alberton, P., Foehr, P., Burgkart, R., Aszodi, A., Clausen-Schaumann, H., Roths, J., 2017. Sensor. Actuator. B 252, 440–449.
Mishra, A., Kumar, J., Melo, J.S., 2017. Biosens. Bioelectron. 87, 332–338.
Quinn, D.M., 1987. Chem. Rev. 87, 955–979.
Rahmani, T., Hajian, A., Afkhami, A., Bagheri, H., 2018. New J. Chem. 42, 7213–7222.
Sharma, A., Jha, R., Gupta, B., 2007. Sensors Journal, IEEE 7, 1118–1129.
Sharma, G., Shrivastav, A.M., Jana, A., Jha, R., 2018. IEEE Photonics Technol. Lett. 30, 1925–1928.
Sharma, G., Shrivastav, A.M., Kumar, A., Jha, R., 2019. Sens. Actuators, A 289, 180–187.
Shrivastav, A.M., Usha, S.P., Gupta, B.D., 2016. Biosens. Bioelectron. 79, 150–157.
Shrivastav, A.M., Usha, S.P., Gupta, B.D., 2017. Biosens. Bioelectron. 90, 516–524.
Shrivastav, A.M., Sharma, G., Rathore, A.S., Jha, R., 2018. ACS Photonics 5, 4402–4412.
Song, B., Cao, W., Wang, Y., 2016. Nanotub. Carbon Nanostructures 24, 435–440.
Tan, Y., Ahmad, I., Wei, T.X., 2015. Chin. Chem. Lett. 26, 797–800.
Tian, Z., Yam, S.S.H., Barnes, J., Bock, W., Greig, P., Fraser, J.M., Loock, H.P., Oleschuk, R.D., 2008. IEEE Photonics Technol. Lett. 20 (8), 626–628.
Tian, X., Liu, L., Li, Y., Yang, C., Zhou, Z., Nie, Y., Wang, Y., 2018. Sensor. Actuator. B 256, 135–142.
Vlatakis, G., Anderson, L.I., Muller, R., Mosbach, K., 1993. Nature 361, 645.
Wang, Q., Wei, W., Guo, M., Zhao, Y., 2016. Sens. Actuators, B 222, 159–165.
Wang, F.R., Lee, G.J., Haridharan, N., Wu, J.J., 2018. Electrocatalysis 9, 1–9.
Wu, B., Hou, L., Du, M., Zhang, T., Wang, Z., Xue, Z., Lu, X., 2014. RSC Adv. 4, 53701–53710.
Zhang, D., Yu, D., Zhao, W., Yang, Q., Kajiura, H., Li, Y., Zhou, T., Shi, G., 2012. Analyst 137, 2629.
Zhou, C., Zou, H., Li, M., Sun, C., Ren, D., Li, Y., 2018. Biosens. Bioelectron. 117, 347–353.